

PROCEEDINGS OF SPIE

[SPIDigitalLibrary.org/conference-proceedings-of-spie](https://spiedigitallibrary.org/conference-proceedings-of-spie)

Defect structure of high-resistivity CdTe:Cl crystals according to the data of high-resolution x-ray diffractometry

Fodchuk, I., Kuzmin, A., Hutsuliak, I., Solodkyi, M., Dovganyuk, V., et al.

I. Fodchuk, A. Kuzmin, I. Hutsuliak, M. Solodkyi, V. Dovganyuk, O. Maslyanchuk, Yu. Roman, R. Zaplitnyy, O. Gudymenko, V. Kladko, V. Molodkin, V. Lizunov, "Defect structure of high-resistivity CdTe:Cl crystals according to the data of high-resolution x-ray diffractometry," Proc. SPIE 11369, Fourteenth International Conference on Correlation Optics, 113691H (6 February 2020); doi: 10.1117/12.2553970

SPIE.

Event: Fourteenth International Conference on Correlation Optics, 2019, Chernivtsi, Ukraine

Defect structure of high-resistivity CdTe:Cl crystals according to the data of high-resolution X-ray diffractometry

I. Fodchuk^a, A.Kuzmin^a, I. Hutsuliak^a, M. Solodkyi^a, V. Dovganyuk^a, O. Maslyanchuk^a, Yu. Roman^a, R. Zaplitnyy^a, O. Gudymenko^b, V. Kladko^b, V. Molodkin^c, V. Lizunov^c

^aChernivtsi National University, Kotsjubynskiyi str. 2, Chernivtsi, Ukraine

^bInstitute of Semiconductor Physics of NASU, Nauky str. 41, Kyiv, Ukraine

^cInstitute for Metal Physics of NASU, Vernadskogo, Blvd. 36, Kyiv, Ukraine

Abstract. The degree of structural perfection of CdTe:Cl single crystals was estimated by methods of high-resolution X-ray diffractometry. Two possible systems of dislocations that consists of two sets of complete 60-degree dislocations and Frank partial dislocations were investigated with the use of Krivoglaz kinematic theory and Monte Carlo method. The density of dislocations that provides correspondence between experimental and simulated reciprocal space maps is determined.

Keywords: cadmium telluride, X-ray multiaxial diffractometry, defect structure, Monte Carlo method, rocking curves, reciprocal space maps.

Igor Fodchuk, E-mail: ifodchuk@ukr.net

1 Introduction

Crystalline cadmium telluride compounds have a wide range of electrophysical properties that have been widely used in recent decades, in particular, they are opaque in visible spectrum and have a significant transmittance (~ 70%) of electromagnetic radiation for wavelengths 2–30 μm . It allows the use of these compounds to design filters for specified spectrum and electron-optical modulators in near and far infrared regions.¹ In addition, cadmium telluride is a promising material for fabrication of solar cells and solar cells based on CdTe with an efficiency of up to 16.5% are today an alternative to Si and GaAs-based structures.^{2,3}

Cadmium telluride has the Gunn effect similarly to gallium arsenide. Although CdTe-based Gunn diodes parameters are slightly worse than GaAs diodes have, but they can be successfully used in certain areas, in particular, to generate microwave oscillations.⁴

Cadmium telluride crystals, doped with chlorine, are promising material for the production of X-wave and γ -radiation detectors.^{5–7} However, the characteristics of such devices are highly dependent on the structural perfection of CdTe crystals.

Cadmium telluride has cubic syngony lattice with the space group $F3m$. It has a sphalerite-type lattice with parameter $a=6,481 \text{ \AA}$ and is polar. In this case, this means that the nuclei of complete dislocations can end in Cd or Te (metallic and non-metallic types) atomic planes. Sphalerite usually has high concentrations of different types of complete and partial dislocations (in particular, Shockley and Frank α - and β -dislocations), whose orientational characteristics can be described with use of Thomson tetrahedron, as also helicoidal dislocations are possible.⁸ Dislocations, due to their specific nature, play an important role in reaction of the material to external stresses⁹ and affect electronic and mechanical properties of devices.

The concentrations of microdefects, their type, as well as the symmetry of the fields of static distortions, created by these defects, are possible to estimate according to the angular distributions of intensity, obtained by the method of three-axis X-ray diffractometry. Information on microdefects is usually found from the "tails" of rocking curves (RCs) and diffraction curves (DCs), which mainly are

formed by the diffuse component of X-radiation.^{10, 11} Central region of rocking curves (FWHM of the peak) contains information on such defects as dislocations and corresponds to the diffuse scattering component from randomly distributed dislocations according to Krivoglaz kinematic theory. The analysis of reciprocal space maps (RSMs) makes it possible to assess qualitatively the degree of defectiveness of the structure.¹² The analysis of RCs and DCs gives an opportunity to obtain quantitative estimates of the degree of structural perfection – dislocation densities, integral and local values of deformation, angular misorientation between individual fragments of structure, and bending radius of atomic planes.^{13,14}

This paper presents the results of investigations of a possible dislocation system in high resistance Cl-doped CdTe single crystals by means of high-resolution X-ray diffractometry and simulation based on Krivoglaz kinematic theory.

2 Experimental investigations

The object of study is a set of single crystal (111) CdTe samples from Acro-rad Co., Ltd, grown by the Bridgman method, with size of $5 \times 5 \times 0,5$ mm³.^{15, 16} Experimental studies were performed using *Panalytical Philips X'Pert PRO* diffractometer with $\text{CuK}\alpha_1$ radiation. The divergence of the primary beam and the angular acceptance of the analyzing crystal used in front of the detector were estimated as $\Delta\alpha_{i,f} \approx 12''$.

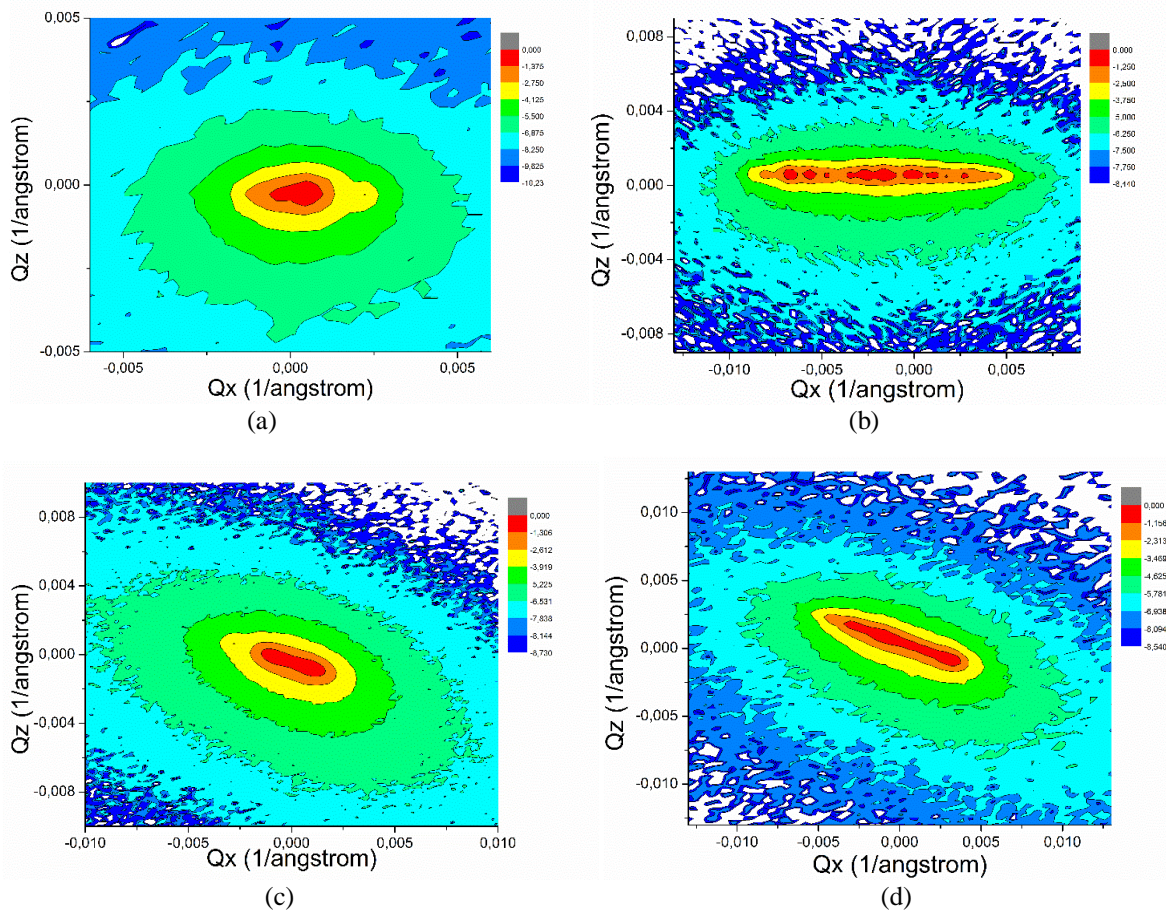


Fig. 1. Experimental $I_h(\omega, 2\theta - \omega)$ distributions; reflexes (333) (a, b) and (331) (c, d); $\text{CuK}\alpha_1$ radiation. Sample №1 – (a, c); sample №2 – (b, d).

The intensity distributions $I_h(\omega)$, $I_h(2\theta - \omega)$ and $I_h(\omega, 2\theta - \omega)$ in Figures 1 and 2 (θ is diffraction angle) are obtained using symmetric and asymmetric diffraction schemes. Cross sections of RSMs were studied for more detailed analysis of the defective structure of the samples, namely, the intensity distribution in the region of reciprocal space lattice nodes for the cross section, parallel to Q_x axis corresponding to RC, and parallel to Q_z axis for DC.

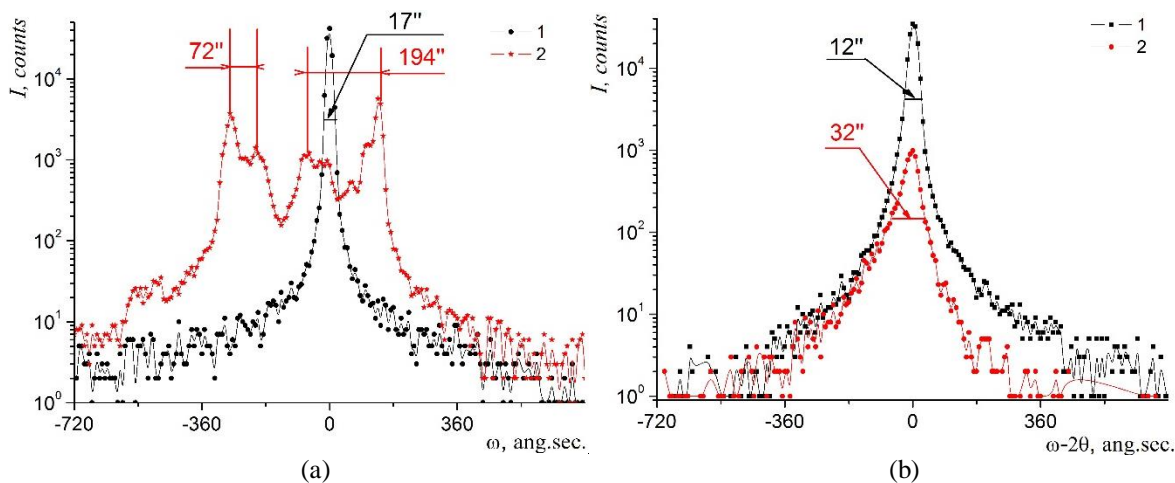


Fig. 2. Experimental $I_h(\omega)$ distributions (RC) (a), $I_h(2\theta - \omega)$ (DC) (b); samples № 1 (1) and № 2 (2); (333) reflex; $\text{CuK}\alpha_1$ radiation.

All studied samples have well-defined defective structure. This is evidenced by the presence of a strong diffuse background from microdefects in $I_h(\omega, 2\theta - \omega)$ distributions and blurring due to the dislocations of quasibragg peaks in $I_h(\omega)$ and $I_h(2\theta - \omega)$ distributions (Fig. 2). The structural perfection of the studied samples was evaluated according to the values of half-width W of quasibragg peak regions (Table 1). The correspondence between the experimental and theoretical values of the half-widths of RC is one of the criteria for assessing the degree of structural perfection of crystals. Analysis of RSM showed that sample №1 is the most perfect in this set (Fig. 1(a)), since the central region is characterized by the smallest value of W along the directions Q_x and Q_z . The presence of additional peaks on RC (Fig. 2(a)) indicates the mosaic structure of the samples, as soon as their intensity and distance between them – the size and angular orientation of grains, respectively.

Table 1. Dislocation densities determined from experimental data (N_G , N_S , N_L) and calculated using the Monte Carlo method (N_F and N_M)

Sample №	reflection	N_G , (cm ⁻²) 10 ⁵	N_L , (cm ⁻²) 10 ⁶	N_S , (cm ⁻²) 10 ⁵	N_F , (cm ⁻²) 10 ⁵	N_M , (cm ⁻²) 10 ⁵
1	333	3,4	–	4,8	2,4	7,2
2		5,8	5,12	4,9	8,2	9,3
3		6,3	4,5	11,32	7,3	8,4
4		2,9	2,1	8,1	1,8	7,8
1	331	1,3	–	–	2,8	7,3
2		13,1	5,58	–	12,3	9,6
3		10,3	4,72	–	11,1	8,6
4		1,3	1,3	–	2,2	7,9

As a rule, significant changes of the shape of RC, which are often observed, are interpreted within the so-called phenomenological model of "blocks" and "distortions" of the lattice.¹⁷ However, this approach is largely formal.

It is known that the contribution to the change in shape and half-width of RC is made by: structural imperfections of the crystal, width of angular intervals of reflection from monochromator and sample, geometric factors.¹⁸ The contribution of each component can be distinguished in different ways. For example, if the shape of RC is described by the Gaussian distribution, then the part of defective component W_G , which depends on the density of dislocations and packaging defects, is determined by the relation

$$W_{\text{exp}} = \sqrt{W_G^2 + W_{\text{teor}}^2}, \quad (1)$$

where $W_{\text{teor}} = \frac{2C|\chi_h|}{\sin 2\theta}$, χ_h is the Fourier component of crystal polarization, C is the polarization factor. In particular, for the symmetric (333) reflex $W_{\text{teor}} = 4''$, and for the asymmetric (331) – $W_{\text{teor}} = 6''$.

Equation (1) allow us to obtain a quantitative estimate of the increase in the half-width of RC (W_G) due to integral effect of various types of defects in crystal. In the case of chaotic distribution of dislocations, which is often found in real crystals, the average dislocation density can be estimated¹⁹ as

$$N_G = \frac{W_G^2}{9|\vec{b}|^2}, \quad (2)$$

where \vec{b} is the Burgers vector of crystal dislocations.

If the crystal consists of blocks separated by small angular boundaries, formed by one dislocation system, then the dislocation density N_L in the direction perpendicular to the dislocation lines can be estimated by the angle $\Delta\theta$ of disorientation between the two blocks¹⁹:

$$N_L = \frac{\Delta\theta}{3|\vec{b}|T} \quad (3)$$

where T is the average block size.

Table 1 shows estimation of N_G for all samples. The value of N_G was determined for the most perfect grain, Since characteristic fragmentary (mosaic) structure appears for samples № 2 and № 3 on $I_h(\omega)$ distributions (Fig. 2). In addition, possible densities N_L of dislocations, located at the boundaries of grains, were also taken into account for specimens № 2, № 3 and № 4 (Table 1). At the same time, Table 1 also shows the possible densities N_S of screw dislocations, which were estimated from the Williamson-Hall plot by the slope angle α of mosaic grains (Fig. 3)^{20, 21}:

$$N_S = \frac{\alpha^2}{4,35*|\vec{b}|^2} \quad (4)$$

The values N_G and N_S obtained in Table 1 confirm that sample №1 is the most perfect, sample №2 is the least perfect, and samples №3 and №4 occupy an intermediate position. They are characterized by complex fragmentary (mosaic) structure and considerable dislocation densities.

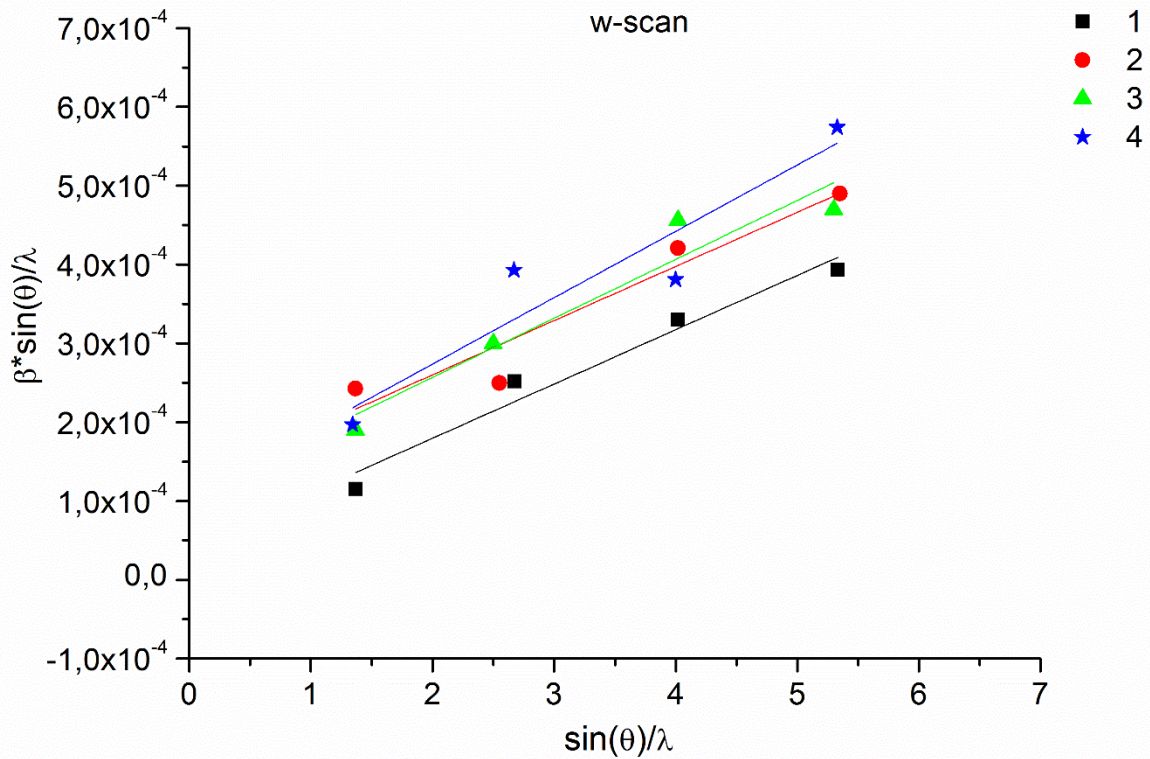


Fig. 3. Williamson-Hall plot for a series of symmetric (hhh) reflexes of ω -scans for evaluation of N_S in samples №1-№4.

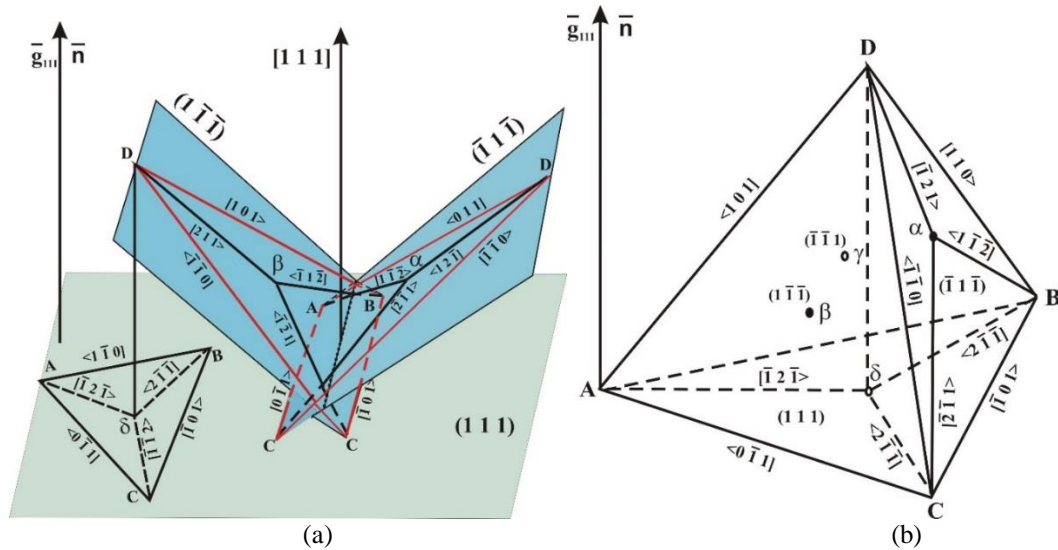


Fig. 4. (a) Schematic layout of two dislocation systems with Burgers vectors and lines located in $(\bar{1}\bar{1}\bar{1})$ and (111) planes (a); Thomson tetrahedron and dissociation of complete dislocations CD and DB on partial Shockley dislocations Da and aC, vertex dislocation BC, and CD on Frank D δ and Shockley δ C dislocations (b).²⁵

In general, cadmium telluride crystals, in addition to dislocations, are characterized by the presence of a whole spectrum of microdefects, inclusions of another phase, stoichiometry disturbances, etc. Such defects are usually evidenced by asymmetry in the form of RC, namely of their tails. In this case, the analysis of the diffuse scattering component allows us to estimate the size and concentration of microdefects.²²

At the same time, it is of great interest to study the influence of the dislocation system on the increase in the values of widths W and the influence of X-ray scattering effects on the shape of RSMs and RCs, using theoretical concepts developed in works²³ and²⁴.

It should be noted that the orientational characteristics of the Burgers vectors of dislocations in corresponding $\{111\}$ planes for CdTe are described by the Thomson tetrahedron.²⁶⁻²⁸ Figure 4 shows probable dissociation of complete 60-degree CD and DB dislocations to partial with next Burgers vectors: Frank edge dislocations $\vec{b}_F = a/3 \langle 111 \rangle$; Shockley screw dislocations $\vec{b}_S = a/6 \langle 112 \rangle$; vertex edge dislocations $\vec{b}_V = a/6 [\bar{1}01]$ and Lomer-Cottrell dislocation barriers, consisting of one vertex and two Shockley dislocations. In particular, in Fig. 4(b):

$$a/2 [011] \rightarrow a/6 [1\bar{1}2] + a/6 [\bar{1}2\bar{1}] \quad (5)$$

$$a/2 [011] + a/2 [\bar{1}\bar{1}0] \rightarrow a/6 [\bar{1}21] + a/6 [\bar{1}\bar{2}1] + a/6 [\bar{1}01] \quad (6)$$

$$a/2 [011] + a/2 [0\bar{1}1] \rightarrow a/6 [\bar{1}12] + a/6 [1\bar{1}2] + a/3 [001] \quad (7)$$

It is known that vacancies can form a disk, whose flat surfaces are $\{111\}$ planes. If the disk is slammed with displacement of flat surfaces along the direction, perpendicular to the surface, then a Frank-type dislocation loop, which limits the packing defect of the full type, is created.

3 Theoretical relations

Different approaches of kinematic (Krivoglaz theory²⁹) and dynamic diffraction theories³⁰⁻³² can be used to simulate RSMs.

If one limits himself to the case of distortions, when atomic planes are displaced relatively to the positions in ideal crystal without changing their scattering ability, then the polarization of the real crystal $\chi(\mathbf{r})$ can be decomposed into a Fourier series^{33, 34}

$$\chi(\vec{r}) = \sum_{\mathbf{g}} \chi_{\mathbf{g}}(\vec{r}) e^{i\vec{g}(\vec{r} - \delta\vec{u}(\mathbf{r}))} = \sum_{\mathbf{g}} \chi_{\mathbf{g}}(\vec{r}) e^{i\vec{g}_{\text{def}}(\vec{r} - \delta\vec{u}(\mathbf{r}))}, \quad (8)$$

where \vec{g} is the reciprocal lattice vector, $\chi_{\mathbf{g}}(\vec{g})$ is the g th component of Fourier polarization, $\vec{u}(\mathbf{r})$ is the field of random displacements in crystal, in particular:

$$\vec{u}(\mathbf{r}) = \langle \vec{u}(\mathbf{r}) \rangle + \delta\vec{u}(\mathbf{r}), \vec{g}_{\text{def}} = \vec{g} - \nabla(\vec{g} \cdot \langle \vec{u}(\mathbf{r}) \rangle). \quad (9)$$

Here \vec{g}_{def} is a vector of averaged reciprocal lattice. In the following we denote "def".

In the presence of a high concentration of dislocations in crystals, a complete differential scattering cross section (coherent + diffuse components) will be³⁵

$$\frac{d\sigma}{d\Omega} = \frac{K^4}{16\pi^4} |\chi_{\mathbf{g}}|^2 \iiint d^3\vec{r} \iiint d^3\vec{r}' G_{\mathbf{g}}(\vec{r}, \vec{r}') e^{-i\mathbf{g}(\vec{r} - \vec{r}')} \quad (10)$$

where V is the volume of the sample, Ω is the form function and the Green function $G_{\mathbf{g}}$ is

$$G_{\mathbf{g}}(\vec{r}, \vec{r}') = \langle e^{-i\mathbf{g}(\vec{u}(\vec{r}) - \vec{u}(\vec{r}'))} \rangle \equiv e^{-T_{\mathbf{g}}(\vec{r}, \vec{r}')}, \text{ a } \vec{u}(\vec{r}_n) \equiv \vec{u}_n = \sum_{\alpha} \sum_m c_m^{\alpha} \vec{v}_{nm}^{\alpha}. \quad (11)$$

Here c^{α} is the concentration of α -type dislocations, \vec{v}^{α} is the displacement field from α -type dislocations, T is scattering operator, which in the kinematic approximation is $T \approx V$, where V is the scattering potential.

In the kinematic approximation of the scattering theory, amplitude of coherent part of scattered

wave is proportional to

$$\langle E \rangle_{\infty} \iiint d^3\vec{r} \langle \chi_g(\vec{r}) e^{-ig\delta\vec{u}(\vec{r})} \rangle e^{-ig\vec{r}}. \quad (12)$$

If sample is statistically homogeneous, then

$$\langle \chi_g(\vec{r}) e^{-ig\delta\vec{u}(\vec{r})} \rangle = \chi_g e^{-D} \quad (13)$$

where $0 < e^{-D} < 1$ is static Debye-Waller factor.

Usually, dislocations positions in real crystals are highly correlated.^{36, 37} In this case, the expression for T will be

$$T_h(\vec{r}_n, \vec{r}_m) \equiv T_{hnm} = T_{hnm}^{(1)} + T_{hnm}^{(2)}, \quad (14)$$

where

$$T_{hnm}^{(1)} \approx \sum_{\alpha, k} c^{\alpha} \Phi_{nmk}^{\alpha}; \quad \Phi_{nmk}^{\alpha} = 1 - e^{-i\vec{h}(\vec{v}_{nk}^{\alpha} - \vec{v}_{mk}^{\alpha})}; \quad \rho^{\alpha} = c^{\alpha}/a^n \quad (15)$$

is uncorrelated addition, and

$$T_{hnm}^{(2)} \approx -\frac{1}{2} \sum_{(\alpha, k) \neq (\beta, \delta)} \langle \delta c_k^{\alpha} \delta c_s^{\beta} \rangle \Phi_{nmk}^{\alpha} \Phi_{nms}^{\beta}, \quad \delta c_k^{\alpha} = c_k^{\alpha} - c^{\alpha} \quad (16)$$

includes two-point correlation, described by correlation function

$$\varepsilon_{ks}^{\alpha\beta} = \langle \delta c_k^{\alpha} \delta c_s^{\beta} \rangle, \quad (17)$$

where n is a dimension of dislocation array, ρ^{α} is n -dimensional dislocation density, and it is also assumed that $c^{\alpha} \ll 1$.

Within this theory, using the Monte Carlo method, based on relations (14)–(17), one can calculate the intensity of scattered radiation $I(Q_x, Q_z)$ in the case of a possible dislocation system in cadmium telluride crystals.³⁸

4 Simulation results

In our case, simulation of RSMs (Fig. 5) was performed using relations (8)–(17) of kinematic Krivoglaз theory²⁹, which well describes coherent and diffuse scattering of X-waves in crystals that contain high concentrations of screw and edge dislocations. Since the dislocation density in the crystals is quite high ($\sim 10^5$ – 10^6 cm^{-2}), the Monte Carlo method was used to simulate RSMs taking into account relaxation of surface stresses (Fig. 5).

Two model systems of dislocations were selected to determine the influence of structure imperfections on the formation of RSMs: a) complete 60-degree dislocations with Burgers vectors $\vec{b}_1 = a/2 [\bar{1}\bar{1}0]$ and $\vec{b}_2 = a/2 [011]$, whose lines are in $(1\bar{1}\bar{1})$ and $(\bar{1}1\bar{1})$ planes (Fig. 4a); b) partial Frank dislocations $\vec{b}_F = a/3 < 111 >$, whose lines are oriented in $< 0\bar{1}1 >$ and $[\bar{1}01 >$ directions (Fig. 4(b)). Such dislocations may also be located within low-angle boundaries between blocks.³⁹

Monte Carlo calculations were performed until coincidence of half-widths of experimental and theoretically calculated distributions of RSMs along Q_x and Q_z directions for symmetric and asymmetric reflexes (Fig. 5). The densities N_M and N_F of complete and partial dislocations of two model systems, determined during the simulation process, are different (Table 1). This may be due to the choice of geometry of the dislocation systems, and obviously to different influence of screw and edge components of complete and partial dislocations, as well as to the fact that the influence of dislocations located at the boundaries of grains has been partially taken into account.

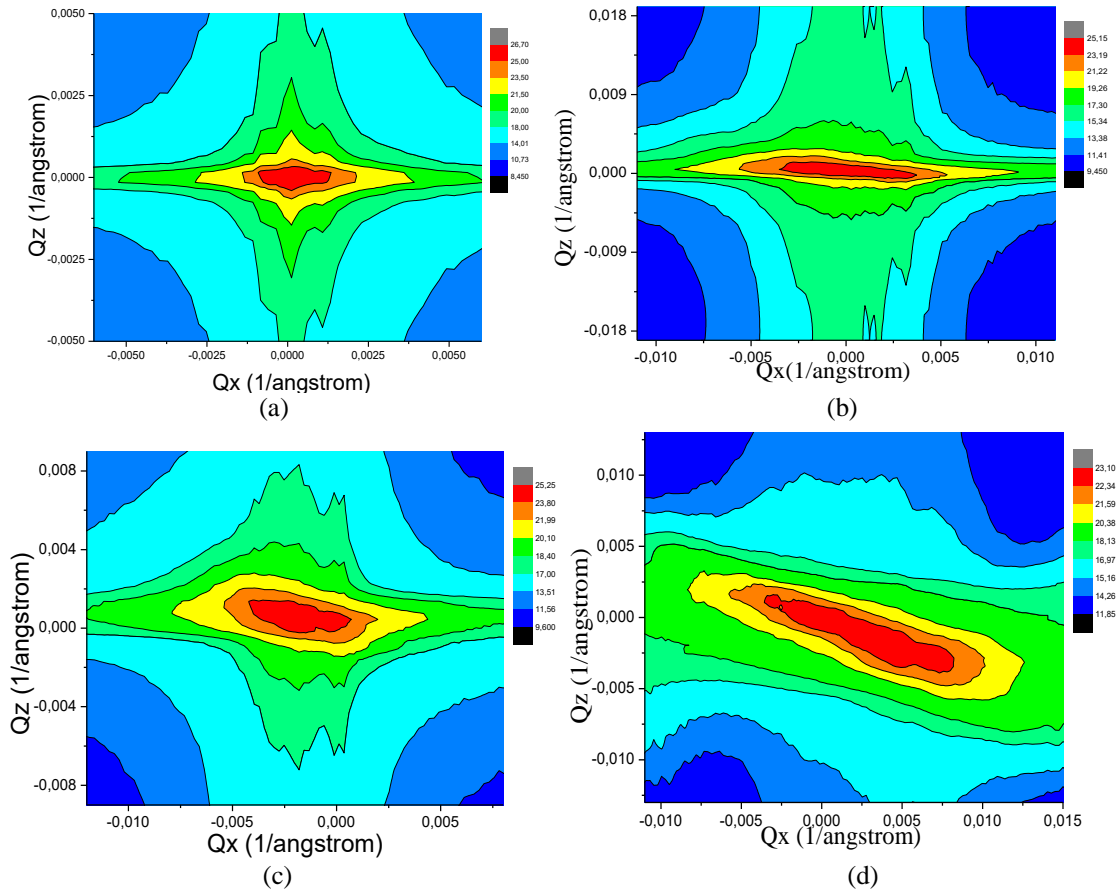


Fig. 5. Simulated $I_h(Q_x, Q_z)$ distributions, (333) and (331) reflexes, $\text{CuK}\alpha_1$ radiation, samples №1 (a, c) and №2 (b, d).

Calculated N_M values are higher than the experimental ones for the first model. Probably, in the case of symmetric diffractions, both screw components of 60-degree dislocations (in particular, partial Shockley dislocations $\vec{b}_S = a/6 < 112 >$) and edge components (Frank dislocations $D\delta$ (Fig. 4)), whose components of Burgers vectors $\vec{b}_F = a/3 [111]$ are parallel to the diffraction vector \vec{g} . Vertex edge dislocations can also contribute to the formation of RSMs of asymmetric (331) diffraction.

The best correspondence of calculated N_F values with the experimental ones is obtained from the model of two sets of partial Frank dislocations (Table 1). It should be noted that such defects are characteristic for CdTe.⁴⁰

At the same time, not only the possible dynamic processes of X-ray scattering, but also more complex, characteristic for CdTe defect structure, must be taken into account for a more complete coincidence of experimental and simulated RSMs, especially of the areas of diffuse scattering.

Conclusions

1. The degree of structural perfection of CdTe:Cl single crystals was estimated with use of high-resolution X-ray diffractometry. A possible dislocation structure in CdTe single crystals has been experimentally and theoretically investigated, and its effect on the formation of RSMs has been analyzed.

2. Estimates of dislocation densities N_G , obtained from the analysis of the FWHM values of experimental rocking curves, as well as N_S , obtained from Williamson-Hall plot as a function of the slope angle α , are shown. The most perfect crystal has the dislocation density within 10^5 cm^{-2} . Other samples have a complex mosaic structure and considerable dislocation densities $\sim 10^6 \text{ cm}^{-2}$.

3. A model dislocation system of two sets of dislocations was investigated on the basis of Krivoglaz kinematic theory and using the Monte Carlo method: 60-degree dislocations with Burgers vectors $\vec{b}_1 = a/2 [\bar{1}\bar{1}0]$ and $\vec{b}_2 = a/2 [011]$, whose lines are in $(1\bar{1}\bar{1})$ and $(\bar{1}1\bar{1})$ planes; partial Frank dislocations $\vec{b}_F = a/3 \langle 111 \rangle$, whose lines are oriented in $\langle 0\bar{1}1 \rangle$ and $[\bar{1}01 \rangle$ directions. The calculations were performed till the coincidence of FWHM of experimental and theoretically calculated intensity distributions of RSMs along Qx and Qz directions for symmetric and asymmetric reflexes. The best fit of calculated dislocation densities with experimental ones is given by a model representation of two sets of partial Frank edge dislocations.

4. At the same time, dynamic processes of coherent and diffuse X-ray scattering, as well as a more complex structure with a whole spectrum of high microdefect concentrations (with spherical, cylindrical or prismatic shapes), need to be taken into account in order to achieve a more complete correspondence between experimental and theoretical RSMs, especially of the diffuse scattering regions.

References

1. N. Armani and C. Ferrari, "Defect-induced luminescence in high – resistivity high-purity undoped CdTe crystals," *Phys. Condens. Matter.* **14**, 13203–13209 (2002).
[doi:10.1088/0953-8984/14/48/369]
2. A. Romeo, "Growth and characterization of high efficiency CdTe/CdS solar cells," *diss. doctor of natural sciences*, Zurich. (2002).
3. X. Wu, "High-efficiency polycrystalline CdTe thin-film solar cells," *Solar Energy.* **6**(77), 803–814 (2004).
[doi:10.1016/j.solener.2004.06.006]
4. Y. Eisen, A. Shor and I. Mardor, "CdTe and CdZnTe and $\text{Cd}_{1-x}\text{Zn}_x\text{Te}$ gamma-ray detector for medical and industrial imaging system," *Nuclear Instruments and Methods in Physics Research Section A: Accelerators, Spectrometers, Detectors and Associated Equipment.* **428**(1), 158-170 (1999).
[doi:10.1016/S0168-9002(99)00003-0]
5. C. Scheiber, and G.C. Giakos, "Medical applications of CdTe and CdZnTe detectors," *Nuclear Instruments and Methods in Physics Research Section A: Accelerators, Spectrometers, Detectors and Associated Equipment.* **458**(1-2), 12-25 (2001).
[doi:10.1016/S0168-9002(00)01032-9]
6. J. Franc et al., "CdTe and CdZnTe crystals for room temperature gamma-ray detectors," *Nuclear Instruments and Methods in Physics Research Section A: Accelerators, Spectrometers, Detectors and Associated Equipment.* **434**(1), 146-151 (1999).
[doi:10.1016/S0168-9002(99)00448-9]
7. M. Avenel et al., "Development and characterization of a 3D CdTe:Cl semiconductor detector for medical imaging," *Nuclear Instruments and Methods in Physics Research Section A: Accelerators, Spectrometers, Detectors and Associated Equipment.* **671**(11), 144–149 (2012).
[doi:10.1016/j.nima.2011.11.058]
8. J. Weertman, "Helical Dislocations," *Physical Review.* **107**(5), 1259-1261 (1957).
[doi:10.1103/PhysRev.107.1259]
9. A. Orlova, and B. Sieber, "Dislocations in CdTe plastically deformed at room temperature," *Acta metal.* **32**(7), 1045-10521 (1984).
[doi:10.1016/0001-6160(84)90007-5]

10. M. Azoulay et al., "Crystalline perfection of melt-grown CdTe," *Journal of Crystal Growth*. **101**(1-4), 256-260 (1990).
[doi:10.1016/0022-0248(90)90977-S]
11. K. Lischka et al., "X-ray rocking curves from (100) and (111) CdTe grown on (100) GaAs by hot wall epitaxy," *Appl. Phys. Lett.* **55**(13), 1309-1311 (1989).
[doi:10.1063/1.101640]
12. M. Polat et al., "Reciprocal space mapping study of CdTe epilayer grown by molecular beam epitaxy on (211)B GaAs substrate," *Mater. Res. Express*. **4**(3), 035904 (2017).
[doi:10.1088/2053-1591/aa61b8]
13. D.K. Bowen, B.K. Tanner, *High Resolution X-ray Diffractometry and Topography*, Taylor & Francis (1998).
14. C. Schumacher et al., "X-ray diffraction study and Monte Carlo simulation of the relaxation behavior of epitaxially grown wire structures," *Journal of Applied Physics*. **95**(10), 5494-5497 (2004).
[doi:10.1063/1.1664020]
15. H. Shiraki et al., "THM growth and characterization of 100 mm diameter CdTe single crystals," // *IEEE Trans. Nucl. Sci.* **56**(4), 1717-1723 (2008).
[doi:10.1109/NSSMIC.2008.4775138]
16. H. Shiraki et al., "Improvement of the productivity in the THM growth of CdTe single crystal as nuclear radiation detector," *IEEE Trans. Nucl. Sci.* **57**(1), 395-399 (2010).
[doi:10.1109/TNS.2009.2035316]
17. P. A. Pramod, Ya. Hatwalne and N. V. Madhusudana, "A phenomenological model for the undulating twist grain boundary-C* phase," *Journal Liquid Crystals*. **28**(4), 525-533 (2001).
[doi:10.1080/02678290010018033]
18. X. Chut, B.K. Tanner, "Double crystal X-ray rocking curves of multiple layer structures," *Semicond. Sci. Tech.* **2**, 765-771 (1987).
[doi:10.1088/0268-1242/2/12/002]
19. P.B. Hirt, *Mosaic structure*, Metallurgy, Moscow (1960).
20. E. Schafner, M. Zehetbauer, and T. Ungar, "Measurement of screw and edge dislocation density by means of X-ray Bragg profile analysis," *Materials Science and Engineering*. **319-321**, 220-223 (2001).
[doi:10.1016/S0921-5093(01)00979-0]
21. E. Metzger, R. Hopler, and E. Born, "Defect structure of epitaxial GaN films determined by transmission electron microscopy and triple-axis X-ray diffractometry," *Philosophical Magazine*. **77**(4), 1013-1025 (1998).
[doi:10.1080/01418619808221225]
22. I. Booker et al., "Dislocation density assessment via X-ray GaN rocking curve scans," *Phys. Status Solidi C*. **7**(7-8) 1787-1789 (2010).
[doi:10.1002/pssc.200983615]
23. A. J. McGibbon, S. J. Pennycook, and J. E. Angelo, "Direct Observation of Dislocation Core Structures in CdTe/GaAs (001)," *Science*. **269**(5223), 519-521 (1995).
[doi:10.1126/science.269.5223.519]
24. F. Székely, I. Groma, and J. Lendvai, "Statistic properties of dislocation structures investigated by X-ray diffraction," *Materials Science and Engineering A*. **309-310**, 352-355 (2001).
[doi:10.1016/S0921-5093(00)01629-4]
25. Y.T. Zhu et al., "Dislocation-twin interactions in nanocrystalline fcc metals," *Acta Materialia*. **59**(2), 812-821 (2011).
[doi:10.1016/j.actamat.2010.10.028]
26. H.-J. Lee and B.D., "Molecular dynamics simulation of the interaction between a mixed dislocation and a stacking fault tetrahedron," *Journal Philosophical Magazine*. **89**(9), 821-841 (2009).
[doi:10.1080/14786430902776954]

27. V.M. Shcherbak, I.M. Fodchuk, and V.M. Tikhonova, "Impurity structural defects in CdTe single crystals," *Crystallography*. **36**(6), 1521-1526 (1991).
28. T. Paulauskas et al., "Atomic scale study of polar Lomer–Cottrell and Hirth lock dislocation cores in CdTe," *Acta Crystallographica Section A*. **70**(6), 524-531 (2014).
[doi:10.1107/S2053273314019639]
29. M.A. Krivoglaz, *X-Ray and Neutron Diffraction in Nonideal Crystals*, Springer, Berlin (1996).
30. A. Authier, *Dynamical Theory of X-Ray Diffraction*, Oxford University Press (2001).
31. L. I. Datsenko, V. B. Molodkin, M. E. Osinovsky, *Dynamic scattering of X-rays by real crystals*, Naukova Dumka, Kiev (1988).
32. S. Takagi, "A Dynamical Theory of Diffraction for a Distorted Crystal," *J. Phys. Soc. Jpn.* **26**(5), 1239 (1969).
[doi:10.1143/JPSJ.26.1239]
33. V. B. Molodkin et al., "Dynamical Theory of Triple-Crystal X-Ray Diffractometry and Characterization of Microdefects," *Metallofiz. Noveishie Tekhnol.* **38**(1)99-139 (2016).
[doi:10.15407/mfint.38.01.0099]
34. Y. I. Nesterets and V. I. Punegov, "The statistical kinematical theory of X-ray diffraction as applied to reciprocal-space mapping," *Acta Cryst A*. **56**(6), 540-548 (2000).
[doi:10.1107/S010876730000996X]
35. Z. Swiatek, and I.M. Fodchuk, "X-ray topography of the subsurface single-crystal layers in a skew asymmetric pattern of diffraction in the reflection geometry," *Archives of Metallurgy and Materials*. **61**(4), 1931-1938 (2016).
[doi:10.1515/amm-2016-0310]
36. Z. Swiatek, I. Fodchuk, and R. Zaplitnyy, "Direct and Inverse Problems in X-ray Three-crystal Triple Laue case X-ray topography of subsurface crystal layers," *Journal of Applied Crystallography*. **50**(3), 727-733 (2017).
[doi:10.1107/S1600576717007208]
37. A.A.Al-Ghamdi et al., "Synthesis and optical characterization of nanocrystalline CdTe thin films," *Optics & Laser Technology*. **42**(8), 1181-1186 (2010).
[doi:10.1016/j.optlastec.2010.03.007]
38. V. M. Kaganer, and K. K. Sabelfeld, "X-ray diffraction peaks from partially ordered misfit dislocations," *Physical Review B*. **80**(18), 184105 (2009).
[doi:10.1103/PhysRevB.80.184105]
39. M. Inoue, I. Teramoto, and Sh. Takayanagi, "Cd and Te Dislocations in CdTe," *Journal of Applied Physics*. **34**(2), 404 (1963).
[doi:10.1063/1.1702621]
40. Chen Li et al., "From atomic structure to photovoltaic properties in CdTe solar cells," *Ultramicroscopy*. **134**, 113-125 (2013).
[doi:10.1016/j.ultramic.2013.06.010]

Caption List

Fig. 1. Experimental $I_h(\omega, 2\theta - \omega)$ distributions; reflexes (333) (*a, b*) and (331) (*c, d*); $\text{CuK}_{\alpha 1}$ radiation. Sample №1 – (*a, c*); sample №2 – (*b, d*).

Fig. 2. Experimental $I_h(\omega)$ distributions (RC) (*a*), $I_h(2\theta - \omega)$ (DC) (*b*); samples № 1 (*1*) and № 2 (*2*); (333) reflex; $\text{CuK}_{\alpha 1}$ radiation.

Fig. 3. Williamson-Hall plot for a series of symmetric (*hhh*) reflexes of ω -scans for evaluation of N_s in samples №1-№4.

Fig. 4. (a) Schematic layout of two dislocation systems with Burgers vectors and lines located in $(\bar{1}\bar{1}\bar{1})$ and $(1\bar{1}\bar{1})$ planes (*a*); Thomson tetrahedron and dissociation of complete dislocations CD and DB on partial Shockley dislocations $D\alpha$ and αC , vertex dislocation BC, and CD on Frank $D\delta$ and Shockley δC dislocations (*b*) [41].

Fig. 5. Simulated $I_h(Q_x, Q_z)$ distributions, (333) and (331) reflexes, $\text{CuK}_{\alpha 1}$ radiation, samples №1 (*a, c*) and №2 (*b, d*).

Table 1. Dislocation densities determined from experimental data (N_G, N_S, N_L) and calculated using the Monte Carlo method (N_F and N_M).